

Spontaneous supercurrents and vortex depinning in two-dimensional arrays of φ_0 Josephson junctions

S. Reinhardt^{1,2}, A. G. Penner,³ J. Berger,¹ C. Baumgartner,¹ S. Gronin,⁴ G. C. Gardner⁴, T. Lindemann^{1,4,5}, M. J. Manfra^{1,4,5,6,7}, L. I. Glazman,⁸ F. von Oppen^{1,3}, N. Paradiso^{1,*}, and C. Strunk¹

¹Institut für Experimentelle und Angewandte Physik, University of Regensburg, 93040 Regensburg, Germany

²School of Applied and Engineering Physics, Cornell University, Ithaca, New York 14853, USA

³Dahlem Center for Complex Quantum Systems and Fachbereich Physik, Freie Universität Berlin, 14195 Berlin, Germany

⁴Birck Nanotechnology Center, Purdue University, West Lafayette, Indiana 47907, USA

⁵Department of Physics and Astronomy, Purdue University, West Lafayette, Indiana 47907, USA

⁶School of Materials Engineering, Purdue University, West Lafayette, Indiana 47907, USA

⁷Elmore Family School of Electrical and Computer Engineering, Purdue University, West Lafayette, Indiana 47907, USA

⁸Department of Physics, Yale University, New Haven, Connecticut 06520, USA



(Received 21 June 2024; revised 27 August 2025; accepted 4 November 2025; published 1 December 2025)

Two-dimensional arrays of ballistic Josephson junctions are important as model systems for synthetic quantum materials. Here, we investigate arrays of multiterminal junctions which exhibit a phase difference φ_0 at zero current. When applying an in-plane magnetic field, we observe nonreciprocal vortex depinning currents. We explain this effect in terms of a ratchetlike pinning potential, which is induced by spontaneous supercurrent loops. Supercurrent loops arise in multiterminal φ_0 junction arrays as a consequence of next-nearest-neighbor Josephson coupling. Tuning the density of vortices to commensurate values of the frustration parameter results in an enhancement of the ratchet effect. In addition, we find a surprising sign reversal of the ratchet effect near frustration 1/3. Our work calls for the search for novel magnetic structures in artificial crystals in the absence of time-reversal symmetry.

DOI: [10.1103/31zv-84hw](https://doi.org/10.1103/31zv-84hw)

I. INTRODUCTION

The magnitude of the maximum supercurrent in Josephson junctions is independent of the polarity of the phase bias when time-reversal or space-inversion symmetry is present. If both symmetries are lifted, the current-phase relation (CPR) is no longer odd under inversion of the phase bias. The first experimental evidence for this asymmetry in an individual junction was the discovery of the anomalous Josephson effect, i.e., a finite phase shift φ_0 of the CPR. Such φ_0 junction behavior has been demonstrated in systems with large spin-orbit interaction (SOI) [1–5]. More recently, similar devices have also featured nonreciprocal critical currents, referred to as the Josephson diode effect [6–14]. As shown in Ref. [15], the anomalous φ_0 shift and Josephson diode effect can coexist in the same device.

With the advent of gate-tunable Josephson junction arrays (JJAs) in super-/semiconducting heterostructures [16], the natural question arises of how two-dimensional (2D) arrays of φ_0 junctions behave. Already in the absence of φ_0 shifts, JJAs are established as an important playground in condensed matter physics. They enable the study of fundamental properties of 2D superconductors in a highly controllable fashion [16] and have been important as model systems for many-body phenomena such as the Berezinski-Kosterlitz-Thouless

transition [17–22], quantum phase transitions [16,23–25], phase locking and synchronized emission [26,27], and macroscopic quantum effects [28–30]. In perpendicular magnetic fields, the resistive state of the arrays is controlled by vortex dynamics. The vortex depinning current displays striking commensurability effects at fractional values of the frustration $f = \Phi/\Phi_0$ [31–34], where Φ is the magnetic flux threading a plaquette and Φ_0 is the superconducting flux quantum.

Introducing and tuning the φ_0 shift by an in-plane magnetic field provides a novel knob for controlling JJAs. For the simplest case of square arrays with nearest-neighbor Josephson coupling only, a uniform φ_0 shift in all junctions can be gauged away and has no experimentally observable consequences. It is an open question as to under which conditions the φ_0 shift has an observable impact on the transport characteristics of JJAs.

Here, we report on two-dimensional square arrays made of φ_0 junctions. Applying an in-plane magnetic field with a component perpendicular to the current, we observe nonreciprocal vortex depinning currents. We make use of this different type of supercurrent diode effect to probe the impact of φ_0 shifts on 2D JJAs. At frustrations $f \ll 1$, the nonreciprocity persists up to fairly large in-plane fields and temperatures. This effect is explained in terms of a field-tunable, ratchetlike shape of the vortex pinning potential, which we deduce from a minimal model of the JJA with both nearest- and next-nearest-neighbor Josephson couplings with anomalous φ_0 shifts. Vortex

*Contact author: nicola.paradiso@physik.uni-regensburg.de

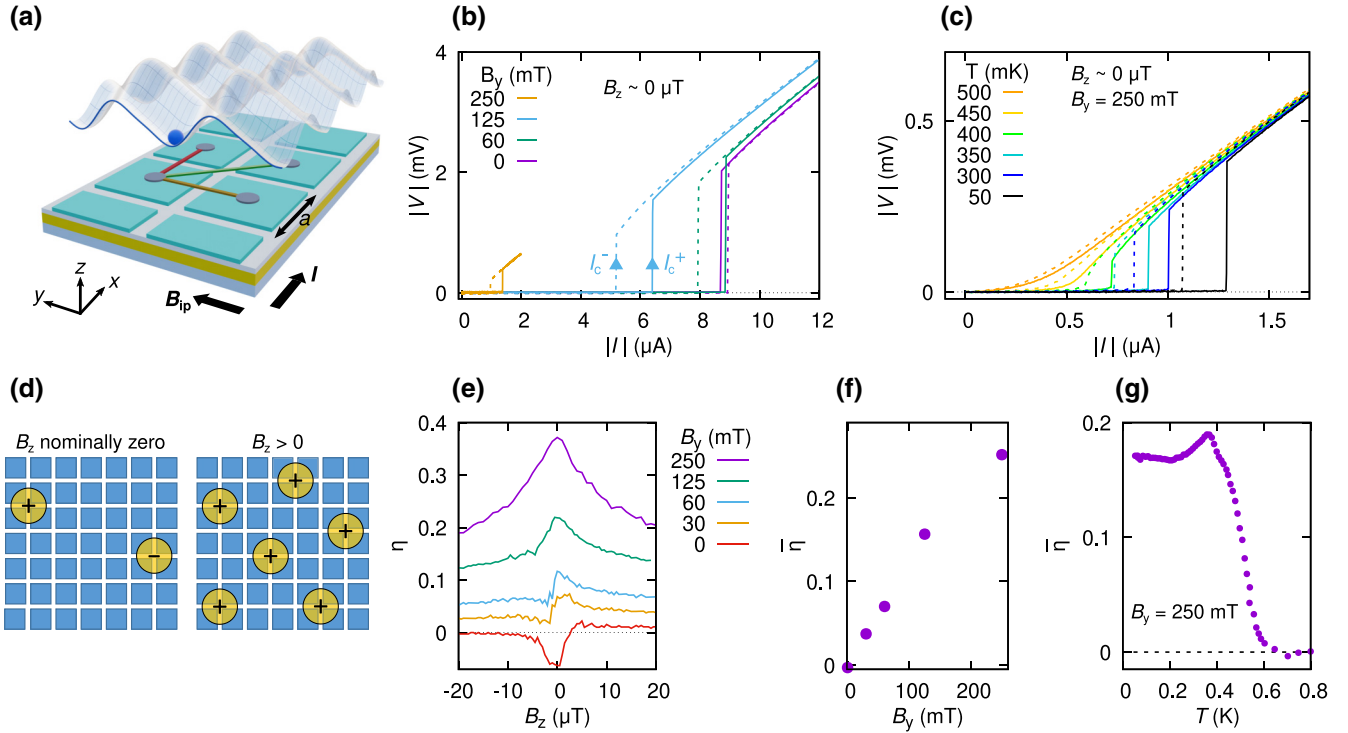


FIG. 1. Nonreciprocal transport in JJs. (a) Two-dimensional square Josephson junction array (JJA) with surface plot showing the vortex pinning potential $U(x, y)$, the bias current I , and the applied in-plane magnetic field B_{ip} . The JJA is modeled using both (red, orange) neighbor and next-nearest- (green) neighbor Josephson couplings between superconducting islands. The lattice constant of the array is $a = 500 \text{ nm}$. (b) Current-voltage characteristics of the 2D JJA for different magnitudes of the in-plane magnetic field. The current is always swept starting at zero absolute value. For the negative branches of the $V(I)$ curves (dotted lines), we plot the absolute values of current and voltage. The out-of-plane magnetic field is close to zero and the temperature is $T \sim 40 \text{ mK}$. (c) Current-voltage characteristics for different temperatures, measured at an in-plane field $B_y = 250 \text{ mT}$. (d) Sketch of vortex configuration at nominally zero out-of-plane magnetic field (left) and positive out-of-plane magnetic field (right). (e) Rectification efficiency $\eta(B_z)$ for $\theta = -90^\circ$ and gate voltage $V_g = 0.5 \text{ V}$, for different values of B_y . (f) Average of η (labeled as $\bar{\eta}$) in the range $|B_z| < 20 \mu\text{T}$ as a function of B_y , extracted from the data shown in (e). (g) Temperature dependence of $\bar{\eta}$ for $B_y = 250 \text{ mT}$, $\theta = -90^\circ$, and gate voltage $V_g = 0.5 \text{ V}$. For $T > 400 \text{ mK}$, there is no well-defined jump in the $V(I)$ curves which can be used to define a critical current. Therefore, we use a threshold $V_c = 30 \mu\text{V}$ to define the critical current.

nonreciprocity also occurs at fractional f , with inverted sign for $f \simeq 1/3$.

In our devices, the 2D electron gas (2DEG) is located in a shallow InGaAs/InAs/InGaAs quantum well, whose characteristics are described in detail in the Supplemental Material [35]. Superconductivity in the 2DEG is introduced by proximity to an epitaxially grown Al film [36]. Using electron-beam lithography followed by selective wet etching of the Al film, we define a square array of 200×200 aluminum islands separated by 100-nm-wide gaps where the aluminum is removed. The islands are $400 \times 400 \text{ nm}^2$ in size. A global top gate allows us to control the electron density in the weak links.

For $\Phi \ll \Phi_0$, the square JJA (lattice constant $a = 500 \text{ nm}$) feature an intrinsic vortex pinning potential—also called egg-crate potential [17]— $U(x, y) \approx E_B[\cos(2\pi x/a) + \cos(2\pi y/a)]$ with minima of the potential located near the corners of the superconducting islands, as illustrated in Fig. 1(a). When applying a transport current with density \vec{j} , vortices experience a Lorentz force $\vec{F}_L = \Phi_0 \vec{j} \times \vec{z}$ perpendicular to the applied current. Depinning of vortices occurs when the Lorentz force exceeds the maximal gradient of the pinning potential. For a single vortex in a square array, the depinning

current density is $j_c = 2\pi E_B/a\Phi_0$, which is approximately 10% of the critical current density of the individual junctions [17,24,37]. Thus, in 2D JJA, as soon as vortices are present, the measured critical current is determined by their depinning threshold and not by the individual junction critical current.

In the present work, we only consider the effects of vortex depinning in the bulk of the JJA. This is justified by using arrays with very large dimension of 200×200 islands, which reduces the role of vortex nucleation and escape at the array edges. In addition, transport properties of very large two-dimensional arrays are less sensitive to disorder, as vortex motion is less affected by single weak junctions with a lower critical current. This is in contrast to our earlier work on one-dimensional arrays of JJs in the same material platform where a single weak junction lowers the total critical current of the whole array [7,38].

II. EXPERIMENTAL RESULTS

Figures 1(b)–1(g) show dc transport data in the regime of very dilute vortices (frustration $f \ll 1$, where $f = B_z/B_0$ with $B_0 = \Phi_0/a^2 = 8.2 \text{ mT}$). Figure 1(b) shows $V(I)$

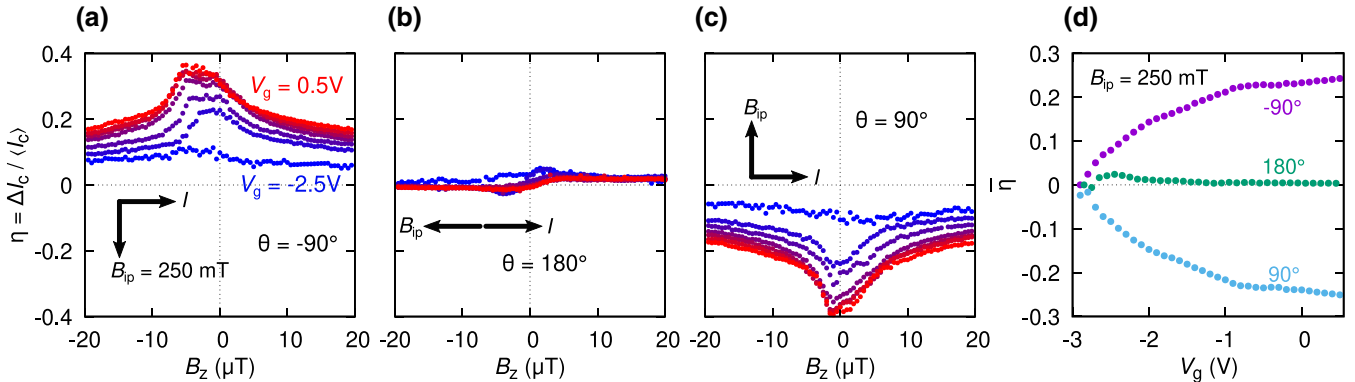


FIG. 2. Tunability of rectification. (a)–(c) Rectification efficiency $\eta = \Delta I_c / I_{c,\text{mean}}$ for different orientations (black arrows) of the in-plane field \vec{B}_{ip} , measured at $B_{ip} = 250\text{ mT}$ and temperature $T \sim 40\text{ mK}$ kept constant during the entire measurement. The color corresponds to different values of the gate voltage V_g , varied in steps of 0.5 V from -2.5 V to 0.5 V . (d) Average of η (labeled as $\bar{\eta}$) in the range $|B_z| < 20\text{ }\mu\text{T}$ at $B_{ip} = 250\text{ mT}$ as a function of gate voltage for different orientations of the in-plane magnetic field.

characteristics for different magnitudes of the in-plane magnetic field which is applied perpendicular to the direction of the transport current. A large difference between positive and negative critical currents is observed for nonzero in-plane fields. While the critical current is strongly reduced at the largest in-plane field of $B_y = 250\text{ mT}$, a sizable asymmetry is still visible. The temperature dependence of $V(I)$ characteristics at $B_y = 250\text{ mT}$ is shown in Fig. 1(c). The nonreciprocity of the $V(I)$ curves persists with increasing temperature until a well-defined critical current is no longer observable at $T \sim 450\text{ mK}$. To quantify the degree of nonreciprocity, Fig. 1(e) shows the rectification efficiency $\eta \equiv (I_c^+ - |I_c^-|)/\langle I_c \rangle$ [with $\langle I_c \rangle \equiv (I_c^+ + |I_c^-|)/2$] as a function of out-of-plane field B_z for different magnitudes of the in-plane field B_y . The central observation is that both the critical current and the rectification efficiency η are even functions of B_z and display a sharp—roughly $10\text{ }\mu\text{T}$ -wide—peak near B_z . Even at nominally $B_z = 0$, the critical current density is about 10 times less than the Josephson junction critical current density. Thus we conclude that the observed switching to the normal state is signaling the depinning of Josephson vortices. The fact that Josephson vortices are present at nominally $B_z = 0$ is not too surprising. A single vortex in our array with size $100 \times 100\text{ }\mu\text{m}^2$ corresponds to a field of 200 nT . The out-of-plane field that we use to compensate the misalignment of the in-plane field always has a finite inhomogeneity in (x, y) . Even a tiny inhomogeneity (sub- μT over hundreds of micrometers) is sufficient to obtain vortices and antivortices somewhere in the array, even though B_z averaged over the array can be accurately set to zero; see sketch in Fig. 1(d), left panel. When discussing our theory model, we shall demonstrate that the spin-orbit-induced rectification efficiency has the same sign for vortices and antivortices [implying that $\eta(B_z)$ is even]. This is a peculiar feature of spin-orbit-induced ratchets which contrasts with the behavior of ratchets demonstrated so far, which are obtained by real-space asymmetry of the potential.

The rectification efficiency η as a function of B_z is shown in Fig. 1(e) for different values of the in-plane field B_y . For large values of $B_y \geq 60\text{ mT}$, we observe symmetric behavior of η around $B_z = 0$, which is expected for a magnetochiral effect driven by the Zeeman field. For lower values of

B_y , we observe an antisymmetric component in $\eta(B_z)$ which is superimposed onto the symmetric magnetochiral effect. Antisymmetric rectification was previously observed for superconducting thin-film devices and is known to originate from device imperfections [39–41]. It is possible that the observed residual antisymmetric rectification is due to a similar mechanism, which is not the focus of the present work. In order to isolate the magnetochiral rectification effect, we average η over the field range $|B_z| < 20\text{ }\mu\text{T}$ ($f < |0.0024|$). This averaged rectification $\bar{\eta}$ is insensitive to the antisymmetric component of the rectification. The resulting plot of $\bar{\eta}(B_y)$ in Fig. 1(f) shows that $\bar{\eta}(B_y)$ increases linearly up to 125 mT and continues to increase with lower slope up to 250 mT . As a function of temperature, $\bar{\eta}$ shows no decrease until the temperature is increased above $T \sim 400\text{ mK}$, as shown in Fig. 1(g). Both observations confirm that the observed rectification efficiency is not related to the single Josephson junction diode effect [7]: in fact, the Josephson diode effect in similar Rashba systems always shows a maximum at roughly 100 mT , followed by a rapid decay [7,12,15,42]. Also, the suppression of higher harmonics (and thus of the diode effect) in such systems is already substantial above 100 mK . On the other hand, the φ_0 shift is expected to grow monotonically and to be nearly constant in temperature [15]. As we shall discuss below, it is precisely the φ_0 shift which induces the nonreciprocal vortex depinning.

If the anomalous Josephson effect is the key for the rectification, we expect a marked dependence of η both on the angle between in-plane field and current, and on the gate voltage controlling the Rashba coefficient and Fermi level. Figures 2(a)–2(c) show η as a function of out-of-plane field B_z and gate voltage for different orientations of \vec{B}_{ip} . The rectification is suppressed when the in-plane field is aligned in the direction of the bias current [except for a residual weak rectification antisymmetric in B_z , which likely has the same origin as the residual rectification at $B_y = 0$ in Fig. 1(e)]. Changing the sign of B_y changes the sign of η . As a function of gate voltage, the averaged rectification efficiency $\bar{\eta}$ monotonically increases with gate voltage [Fig. 2(d)], showing that the nonreciprocity is enhanced by a larger electron density in the weak link. Also the gate dependence of η has a similar behavior as that of φ_0

reported in similar systems [13,15]. The magnitude and sign of the nonreciprocity are reproduced on the nominally identical device B. The measurements on device B are presented in the Supplemental Material, Figs. S7(d) and S7(e) [35]. We have also performed measurements on a JJA (device C) with larger lattice constant $a = 1.1 \mu\text{m}$. In addition, the InAs quantum well of device C has a mean free path of $l_{\max} < 270 \text{ nm}$, which is much lower compared to the mean free path $l_{\max} \sim 700 \text{ nm}$ of the quantum well used for devices A and B. The measurements of device C are presented in Fig. S10 of the Supplemental Material [35]. Our main observation is that the nonreciprocity is much weaker in device C, owing to the larger lattice constant compared to that in devices A and B.

Let us summarize our observations so far: The switch to the normal state is observed at current densities which are one order of magnitude below the expected Josephson critical current density. For example, at low in-plane fields $B_{\text{ip}} \lesssim 100 \text{ mT}$, the critical current density is $j_c \approx 90 \text{ nA}/\mu\text{m}$, while in the case of a ballistic junction, the expected Josephson critical current would be $j_{c,\text{JJ}} = \pi \Delta^*/(eR_N a) \sim 1.9 \mu\text{A}/\mu\text{m}$. Here, we use the measured value $R_N \sim 500 \Omega$ and the estimated induced gap $\Delta^* = 130 \mu\text{eV}$ [38]. Thus, the observed critical currents reasonably agree with the expected vortex depinning currents. The vortex depinning is nonreciprocal if an in-plane field is applied perpendicular to the current. This diode effect shows a gate, temperature, and in-plane field dependence similar to that reported for the φ_0 shift. Finally, $\eta(B_z)$ is even in the out-of-plane field B_z . As mentioned above, a nonreciprocal effect is unexpected for a 2D array of φ_0 junctions when modeling the JJA with a 2D XY model with nearest-neighbor coupling, where islands are linked by junctions in horizontal and vertical directions. However, this model neglects the strong multiterminal character of the junctions in our devices A and B. The magnitude and range of the coupling between islands is ultimately determined by the spatial extent of the Andreev bound states in the proximitized electron gas. The important length scales are the coherence length $\xi_0 = \frac{\hbar v_F}{\pi \Delta^*}$ and the mean free path l_e . From the characterization data (which can be found in the supplemental material of [15]), we deduce a lower bound of 800 nm for ξ_0 (assuming $\Delta^* = 130 \mu\text{eV}$ and $v_F = 5 \times 10^5 \text{ m/s}$) and 250 nm for l_e . Therefore, we can estimate the spatial extent of the Andreev bound states under the Al islands $\xi = \sqrt{\hbar D / \Delta^*} = \sqrt{\xi_0 l_e / 2}$ to be at least 300 nm, which is comparable with the island size. To link the observed nonreciprocal vortex depinning current to the anomalous phase shifts, we transcend the standard XY model with only nearest-neighbor couplings and take the multiterminal character [43,44] of the junctions into account. Microscopically, Andreev bound states (ABSs) in the weak links connect not only nearest-neighbor Al islands, but, to a lesser extent, also next-nearest neighbors, as indicated in Fig. 1(a) (green line). With in-plane magnetic fields along the \hat{y} direction, the diagonal junctions also exhibit a nonzero phase shift φ_0^{diag} , which in general differs from the phase shift φ_0^x of the junctions in the x direction. The additional diagonal couplings render the ground state frustrated even without perpendicular magnetic field: The sums of φ_0 shifts around closed loops no longer cancel. To maintain fluxoid quantization within the plaquettes, spontaneous supercurrents emerge in the ground state; see Figs. 3(a)–3(c). The current

configuration in the ground state has an (up-down) reflection symmetry about the current axis. This symmetry is broken when a vortex is added to the array, as shown in Fig. 3(d). The vortex pinning potential $U(x, y)$ shown on the right side of Fig. 3(d) no longer exhibits fourfold rotational symmetry and $U(x = 0, y)$ exhibits a ratchetlike dependence (see the Supplemental Material for calculation details [35]).

The importance of the diagonal couplings is further emphasized by computing the vortex depinning currents. We minimize the free energy of the JJA with a single vortex located within the array. The depinning current is obtained as the largest bias current, for which the vortex remains localized (for details, see the Supplemental Material [35]). The results are plotted in Fig. 3(e) as a function of the difference $\Delta\varphi_0 = \varphi_0^x - \varphi_0^{\text{diag}}$ between horizontal and diagonal phase shifts. The phase shift affects the depinning currents only when the coupling E_D between next-nearest neighbors is turned on and results in a nonreciprocal depinning current. The corresponding diode efficiencies $\eta \equiv \langle I_c^+ - |I_c^-| \rangle / \langle I_c \rangle$ [with $\langle I_c \rangle \equiv (I_c^+ + |I_c^-|)/2$] are shown in Fig. 3(f) and reach up to 20% for $\Delta\varphi_0 = \pi/2$ and $E_D = 0.8$, comparable to experimental values. Interestingly, in the limit of small frustrations, the nonreciprocal vortex dynamics can be mapped theoretically to the phase dynamics of a single Josephson diode [45]. The motion of an individual vortex along the \hat{y} direction in the pinning potential is governed by the Langevin equation,

$$-\partial_y U - \alpha \dot{y} - \gamma \Phi_0 I = f_y \quad (1)$$

(see Supplemental Material for details, including the geometrical factor γ [35]). The first term describes the pinning force, the second the friction, while the third term corresponds to the Lorentz force exerted by the bias current I in the \hat{x} direction. The Langevin force f_y has zero average and correlator $\langle f_y(t) f_y(t') \rangle = 2\alpha k_B T \delta(t - t')$. Equation (1) maps onto the Langevin equation for the phase difference of a single resistively shunted Josephson junction, with the vortex position becoming the phase difference and the ratchetlike vortex pinning potential turning into the asymmetric current-phase relation.

At this point, we are also able to explain the even dependence of η on B_z . The key idea is that for an antivortex, the potential induced by the spontaneous supercurrents is mirrored in y compared to that for a vortex. This is illustrated in Fig. S4 of the Supplemental Material [35]. Since the direction of the Lorentz force is also opposite, the sign of η remains the same. This behavior is markedly different from the engineered ratchet effect obtained with a real-space asymmetric pinning potential. In that case, the potential is the same for vortices and antivortices, so that the resulting rectification efficiency is opposite. A more detailed discussion of this important point can be found in the Supplemental Material [35].

Beyond the limit of dilute vortices, the rectification coefficient also exhibits interesting behavior at larger frustrations. We probe the vortex dynamics by applying a low-frequency ac current bias with amplitude I_{ac} while measuring the first and second harmonic of resistance using digital lock-in amplifiers. This provides a convenient and fast method to measure the nonreciprocal response [6,46]. The second harmonic of the ac response, $R_{2\omega} \equiv V_{2\omega}/I_{ac}$, becomes nonzero when the amplitude of the ac current is in the rectification window

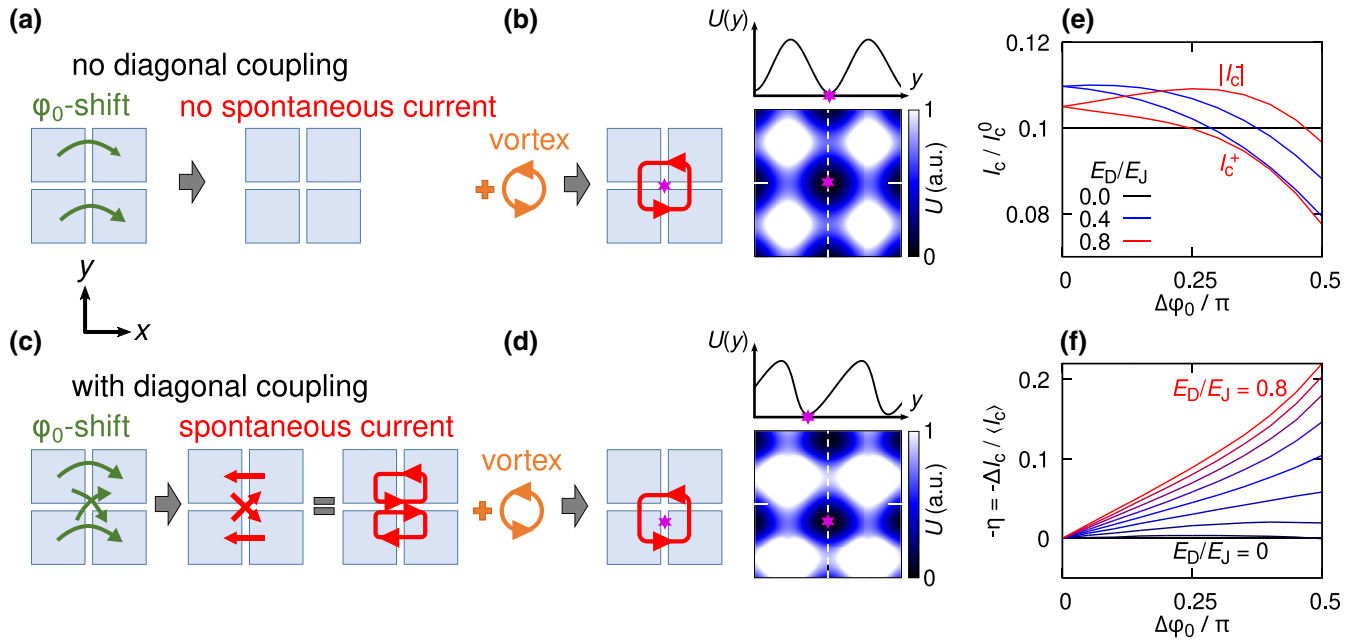


FIG. 3. Model of the ratchet effect. (a) JJA with nearest-neighbor coupling only, with no spontaneous supercurrent in the ground state. (b) Sketch of the Josephson currents for a vortex in the absence of diagonal coupling. The Josephson current distribution remains fourfold symmetric. A color plot of the vortex pinning potential is shown on the right. Vortices driven in the y direction experience a sinusoidal pinning potential $U(y)$, as sketched above the color plot of $U(x, y)$. (c) Anomalous phase shifts $\phi_0^x > \phi_0^{\text{diag}}$ and persistent currents for the case with diagonal coupling. (d) Sketch of the Josephson currents for a vortex in the case with diagonal coupling. The corresponding vortex pinning potential $U(x, y)$ is skewed. Vortices driven in the y direction experience a ratchetlike potential $U(y)$, as sketched above the color plot of $U(x, y)$ [$U(y)$ shown with exaggerated skewness for better visibility]. (e) Numerical simulation of vortex depinning currents. The phase shift parameter $\Delta\phi_0$ is the difference between horizontal and diagonal phase shifts: $\Delta\phi_0 = \phi_0^x - \phi_0^{\text{diag}}$. E_D/E_J is the ratio between diagonal and nondiagonal Josephson couplings. (f) Resulting rectification efficiency $\eta = \Delta I_c / I_c$ extracted from the numerical simulation of positive and negative depinning currents. The diagonal coupling is changed in steps of 0.1 from 0 to 0.8.

($|I_c^-| < I_{ac} < I_c^+$) where $V(I) \neq -V(-I)$. A simulation of $R_\omega(I_{ac})$ and $R_{2\omega}(I_{ac})$ for a current-voltage characteristic with nonreciprocal critical currents is provided in the Supplemental Material [35]. The $R_{2\omega}$ measurement provides better signal-to-noise ratios compared to dc measurements of IV characteristics. Figure 4(a) shows the first harmonic $R_\omega \equiv V_\omega / I_{ac}$ as a function of f and I_{ac} , measured for an in-plane field $B_{ip} = 125$ mT at an angle of $\theta = 90^\circ$ with the applied current \vec{I} . A nonzero resistance is observed when I_{ac} exceeds the vortex depinning current, which strongly depends on the applied out-of-plane field. We observe pronounced maxima of the depinning current for the commensurate values of frustration $f = \pm 1/3, \pm 1/2, \pm 2/3, \pm 1$, where vortices form ordered patterns and pinning is strongly increased [17,47]. It is now interesting to check whether the rectification observed in the dilute vortex limit $f \rightarrow 0$ is also observed for $f > 0$. Figures 4(b) and 4(c) show $R_{2\omega}$ for $\theta = \pm 90^\circ$. First of all, we notice that a significant $R_{2\omega}$ (and thus a rectification) is only observed for some commensurate frustration (e.g., $f = 1/3, 1/2, 1$, etc.), while it is weak for incommensurate f values, namely, outside the peaks. Clearly, the sign of rectification must change sign if B_y changes sign, due to time-reversal symmetry. This is indeed the case, as can be seen by comparing Figs. 4(b) and 4(c). The second important observation is that most of the peaks at finite frustration show the same sign of the rectification as for $f \rightarrow 0$, e.g., negative

in Fig. 4(b) and positive in Fig. 4(c). The third striking observation is the fact that $f = 1/3$ makes an exception since it displays an inverted rectification compared to $f = 0$ and to all other f . Finally, the $f = 2/3$ does not seem to display rectification at all. At present, we do not have a full and comprehensive explanation for the observed phenomenology at finite f . Nonetheless, the following considerations may offer guidance for its interpretation. At finite f , the potential felt by a vortex is not only the native egg-crate potential, but also the potential of interaction with other vortices, which is repulsive for vortices of the same circulation. For incommensurate f , there is no well-defined long-range arrangement of vortices, so we expect no clear ratchet effect averaged over the array scale. At commensurate f , vortices form an ordered pattern, e.g., a checkerboard pattern for $f = 1/2$. The potential felt by a vortex due to the other vortices is thus a 2D periodic potential. However, it is not clear why this potential should show rectification properties. On the other hand, the shape of a vortex (i.e., that of the screening current pattern) might depend on the in-plane field, similarly to what happens to Abrikosov vortices in superconducting films with large spin-orbit interaction [48]. In this case, it is possible that the symmetry of the total egg-crate potential might be reduced, showing ratchet features. Such rectification would then be highly dependent on the specific vortex configuration, and thus on the specific f , so that for some values (2/3) it might disappear or even (1/3)

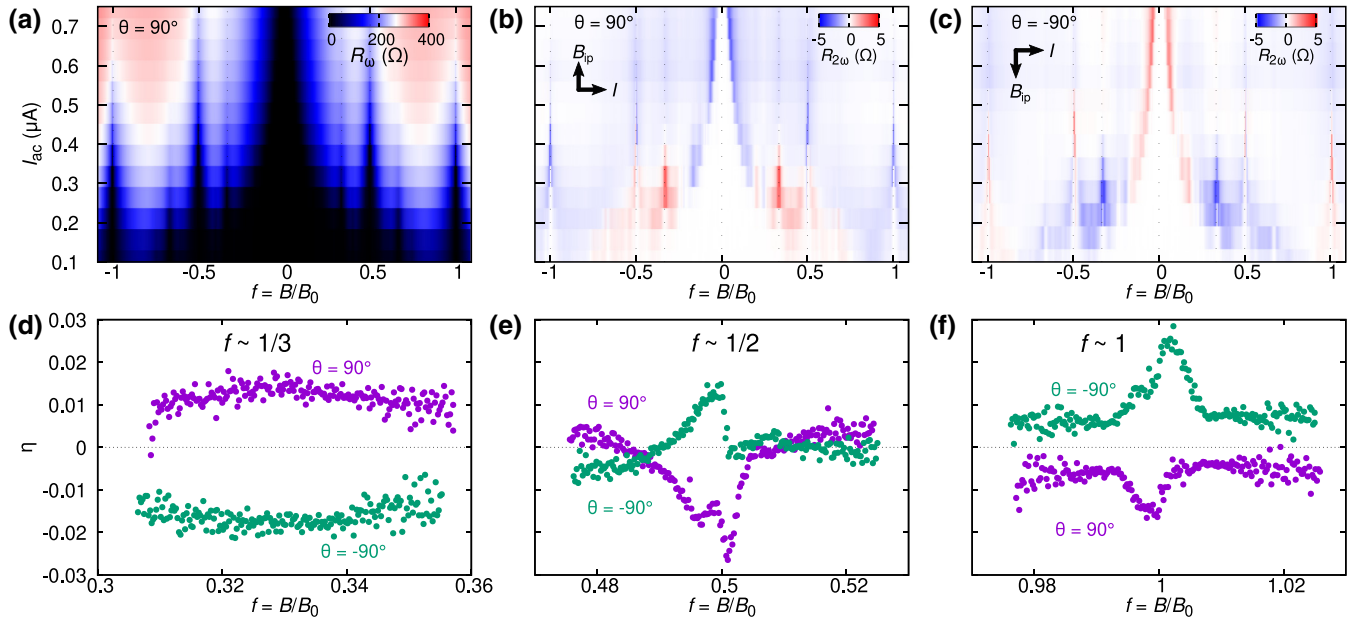


FIG. 4. Ratchet effect at larger frustration. (a)–(c) First harmonic $R_\omega = V_\omega/I_{ac}$ and second harmonic $R_{2\omega} = V_{2\omega}/I_{ac}$ of the resistance measured as a function of frustration and ac bias current. The in-plane field $B_{ip} = 125$ mT is applied perpendicular to the direction of the current. (d)–(f) Rectification efficiency η around commensurate fields $f = 1/3$, $f = 1/2$, and $f = 1$ obtained from standard $V(I)$ transport measurements. In all plots, $T \sim 40$ mK.

change sign. Further theoretical and experimental studies will be required to clarify these aspects.

III. DISCUSSION

We would like to emphasize a key difference between our *magnetochiral ratchet* effect and the vortex ratchet effect reported in previous experiments. So far, a ratchetlike pinning potential was obtained by breaking the real-space symmetry of the system, for example by asymmetrically fabricated pinning sites [49,50]. Here, the array remains fourfold symmetric (D_4 symmetry) and the symmetry of the pinning potential is reduced to that of a ratchet (D_1) by the combination of SOI, Zeeman field, and diagonal couplings. In our magnetochiral ratchets, the rectification efficiency is the same for vortices and antivortices, while it is opposite for asymmetrically fabricated pinning sites [49,50].

A change of sign of the vortex ratchet effect has been previously reported in arrays with asymmetric potential modulation [49–54]. In our case, however, the physics is different: the change of sign we observe is an emergent property of symmetric and periodic arrays, which is evidently related to the particular vortex patterns at commensurate frustration values.

In conclusion, we observe a magnetochiral vortex ratchet effect in 2D arrays of φ_0 junctions. The multiterminal character of our junctions introduces competing φ_0 shifts, leading to frustration and the emergence of spontaneous supercurrent loops in the ground state. These spontaneous currents are ultimately responsible for the nonreciprocity in the depinning current. Our experimental results for $f \ll 1$ are in good agreement with a minimal model for a 2D square array with nearest- and next-nearest-neighbor Josephson couplings, while the sign change at $f = 1/3$ remains an interesting open question.

IV. MATERIALS AND METHODS

Samples are fabricated starting with a heterostructure which is grown by molecular beam epitaxy. The full layer sequence and basic characterization of this heterostructure are presented in the Supplemental Material of our previous work [15]. The top-most layers are a 5 nm film of Al, a 10 nm $\text{In}_{0.75}\text{Ga}_{0.25}\text{As}$ barrier, the 7-nm-thick InAs layer, which hosts the 2DEG, and a 4 nm bottom barrier of $\text{In}_{0.75}\text{Ga}_{0.25}\text{As}$. The devices are structured using standard nanofabrication techniques. Deep etching of the heterostructure is performed using a phosphoric acid solution. The arrays are defined using electron-beam lithography and selective etching of the Al film with transene D.

Transport measurements are performed in a dilution refrigerator with a base temperature of 40 mK. All measurement lines are filtered at room temperature using Pi-type LC filters with a cutoff frequency of 10 MHz. Below the mixing chamber, we use resistive coaxial wires which have a large attenuation at frequencies above 100 MHz. More details of the setup can be found in the Supplemental Material of our previous work [15].

The configuration of vortices in the array and the superconducting contacts will, in general, depend on the history of the out-of-plane magnetic field. Field cooling is required to obtain an equilibrium configuration of vortices. The data presented in the main text have been obtained with the following field-cooling procedures:

- (i) Figure 1(e): field cooling at every value of B_z .
- (ii) All other panels of Figs. 1 and 2: field cooling in nominally zero out-of-plane field before the measurement.
- (iii) Figures 4(a)–4(c): no field cooling.
- (iv) Figures 4(d)–4(f): field cooling at the commensurate fields ($f = 1/3$, $1/2$, and 1) before the measurement.

The full description of the theoretical methods is provided in the Supplemental Material [35].

ACKNOWLEDGMENTS

We thank S. Vaitekenas for fruitful discussions. Work at Universität Regensburg was funded by the EU's HORIZON-RIA Programme under Grant No. 101135240 (JOGATE) and by Deutsche Forschungsgemeinschaft (DFG, German Research Foundation) through Project ID No. 314695032-SFB

1277 (Project No. B08). Research at Freie Universität Berlin was supported through Collaborative Research Center (CRC) 183 (Project No. C03) of the Deutsche Forschungsgemeinschaft and the Einstein Research Unit on Quantum Devices. Research at Yale University was supported by the Office of Naval Research (ONR) under Award No. N00014-22-1-2764 and by the NSF Grant No. DMR-2410182. L.I.G. thanks Freie Universität Berlin for hosting him as a Mercator fellow within CRC 183.

-
- [1] D. B. Szombati, S. Nadj-Perge, D. Car, S. R. Plissard, E. P. A. M. Bakkers, and L. P. Kouwenhoven, Josephson φ_0 -junction in nanowire quantum dots, *Nat. Phys.* **12**, 568 (2016).
- [2] A. Assouline, C. Feuillet-Palma, N. Bergeal, T. Zhang, A. Mottaghizadeh, A. Zimmers, E. Lhuillier, M. Eddrie, P. Atkinson, M. Aprili, and H. Aubin, Spin-orbit induced phase shift in Bi_2Se_3 Josephson junctions, *Nat. Commun.* **10**, 126 (2019).
- [3] W. Mayer, M. C. Dartailh, J. Yuan, K. S. Wickramasinghe, E. Rossi, and J. Shabani, Gate controlled anomalous phase shift in Al/InAs Josephson junctions, *Nat. Commun.* **11**, 212 (2020).
- [4] M. C. Dartailh, W. Mayer, J. Yuan, K. S. Wickramasinghe, A. Matos-Abiague, I. Žutić, and J. Shabani, Phase signature of topological transition in Josephson junctions, *Phys. Rev. Lett.* **126**, 036802 (2021).
- [5] D. Z. Haxell, M. Coraiola, D. Sabonis, M. Hinderling, S. C. ten Kate, E. Cheah, F. Krizek, R. Schott, W. Wegscheider, and F. Nichele, Zeeman- and orbital-driven phase shifts in planar Josephson junctions, *ACS Nano* **17**, 18139 (2023).
- [6] F. Ando, Y. Miyasaka, T. Li, J. Ishizuka, T. Arakawa, Y. Shiota, T. Moriyama, Y. Yanase, and T. Ono, Observation of superconducting diode effect, *Nature (London)* **584**, 373 (2020).
- [7] C. Baumgartner, L. Fuchs, A. Costa, S. Reinhardt, S. Gronin, G. C. Gardner, T. Lindemann, M. J. Manfra, P. E. Faria Junior, D. Kochan, J. Fabian, N. Paradiso, and C. Strunk, Supercurrent rectification and magnetochiral effects in symmetric Josephson junctions, *Nat. Nanotechnol.* **17**, 39 (2022).
- [8] B. Pal, A. Chakraborty, P. K. Sivakumar, M. Davydova, A. K. Gopi, A. K. Pandeya, J. A. Krieger, Y. Zhang, M. Date, S. Ju, N. Yuan, N. B. M. Schröter, L. Fu, and S. S. P. Parkin, Josephson diode effect from cooper pair momentum in a topological semimetal, *Nat. Phys.* **18**, 1228 (2022).
- [9] K.-R. Jeon, J.-K. Kim, J. Yoon, J.-C. Jeon, H. Han, A. Cottet, T. Kontos, and S. S. P. Parkin, Zero-field polarity-reversible Josephson supercurrent diodes enabled by a proximity-magnetized Pt barrier, *Nat. Mater.* **21**, 1008 (2022).
- [10] B. Turini, S. Salimian, M. Carrega, A. Iorio, E. Strambini, F. Giazotto, V. Zannier, L. Sorba, and S. Heun, Josephson diode effect in high-mobility InSb nanoflags, *Nano Lett.* **22**, 8502 (2022).
- [11] S. Ghosh, V. Patil, A. Basu, Kuldeep, A. Dutta, D. A. Jangade, R. Kulkarni, A. Thamizhavel, J. F. Steiner, F. von Oppen, and M. M. Deshmukh, High-temperature Josephson diode, *Nat. Mater.* **23**, 612 (2024).
- [12] A. Costa, C. Baumgartner, S. Reinhardt, J. Berger, S. Gronin, G. C. Gardner, T. Lindemann, M. J. Manfra, J. Fabian, D. Kochan, N. Paradiso, and C. Strunk, Sign reversal of the Josephson inductance magnetochiral anisotropy and 0- π -like transitions in supercurrent diodes, *Nat. Nanotechnol.* **18**, 1266 (2023).
- [13] N. Lotfizadeh, W. F. Schiela, B. Pekerten, P. Yu, B. H. Elfeky, W. M. Strickland, A. Matos-Abiague, and J. Shabani, Superconducting diode effect sign change in epitaxial Al-InAs Josephson junctions, *Commun. Phys.* **7**, 120 (2024).
- [14] A. Banerjee, M. Geier, M. A. Rahman, C. Thomas, T. Wang, M. J. Manfra, K. Flensberg, and C. M. Marcus, Phase asymmetry of Andreev spectra from Cooper-pair momentum, *Phys. Rev. Lett.* **131**, 196301 (2023).
- [15] S. Reinhardt, T. Ascherl, A. Costa, J. Berger, S. Gronin, G. C. Gardner, T. Lindemann, M. J. Manfra, J. Fabian, D. Kochan, C. Strunk, and N. Paradiso, Link between supercurrent diode and anomalous Josephson effect revealed by gate-controlled interferometry, *Nat. Commun.* **15**, 4413 (2024).
- [16] C. G. L. Böttcher, F. Nichele, M. Kjaergaard, H. J. Suominen, J. Shabani, C. J. Palmstrøm, and C. M. Marcus, Superconducting, insulating and anomalous metallic regimes in a gated two-dimensional semiconductor-superconductor array, *Nat. Phys.* **14**, 1138 (2018).
- [17] R. S. Newrock, C. J. Lobb, U. Geigenmüller, and M. Octavio, The two-dimensional physics of Josephson junction arrays, *J. Phys. C* **54**, 263 (2000).
- [18] D. J. Resnick, J. C. Garland, J. T. Boyd, S. Shoemaker, and R. S. Newrock, Kosterlitz-Thouless transition in proximity-coupled superconducting arrays, *Phys. Rev. Lett.* **47**, 1542 (1981).
- [19] D. W. Abraham, C. J. Lobb, M. Tinkham, and T. M. Klapwijk, Resistive transition in two-dimensional arrays of superconducting weak links, *Phys. Rev. B* **26**, 5268 (1982).
- [20] B. J. van Wees, H. S. J. van der Zant, and J. E. Mooij, Phase transitions of Josephson-tunnel-junction arrays at zero and full frustration, *Phys. Rev. B* **35**, 7291 (1987).
- [21] P. Martinoli and C. Leemann, Two-dimensional Josephson junction arrays, *J. Low Temp. Phys.* **118**, 699 (2000).
- [22] R. Cosmic, K. Kawabata, Y. Ashida, H. Ikegami, S. Furukawa, P. Patil, J. M. Taylor, and Y. Nakamura, Probing XY phase transitions in a Josephson junction array with tunable frustration, *Phys. Rev. B* **102**, 094509 (2020).
- [23] H. S. J. van der Zant, W. J. Elion, L. J. Geerligs, and J. E. Mooij, Quantum phase transitions in two dimensions: Experiments in Josephson-junction arrays, *Phys. Rev. B* **54**, 10081 (1996).

- [24] R. Fazio and H. van der Zant, Quantum phase transitions and vortex dynamics in superconducting networks, *Phys. Rep.* **355**, 235 (2001).
- [25] H. Ikegami and Y. Nakamura, Insulating phase in two-dimensional Josephson junction arrays investigated by nonlinear transport, *Phys. Rev. B* **106**, 184511 (2022).
- [26] S. P. Benz and C. J. Burroughs, Coherent emission from two-dimensional Josephson junction arrays, *Appl. Phys. Lett.* **58**, 2162 (1991).
- [27] P. Barbara, A. B. Cawthorne, S. V. Shitov, and C. J. Lobb, Stimulated emission and amplification in Josephson junction arrays, *Phys. Rev. Lett.* **82**, 1963 (1999).
- [28] H. S. J. van der Zant, F. C. Fritschy, T. P. Orlando, and J. E. Mooij, Dynamics of vortices in underdamped Josephson-junction arrays, *Phys. Rev. Lett.* **66**, 2531 (1991).
- [29] W. J. Elion, J. J. Wachters, L. L. Sohn, and J. E. Mooij, Observation of the Aharonov-Casher effect for vortices in Josephson-junction arrays, *Phys. Rev. Lett.* **71**, 2311 (1993).
- [30] P. Delsing, C. D. Chen, D. B. Haviland, Y. Harada, and T. Claeson, Charge solitons and quantum fluctuations in two-dimensional arrays of small Josephson junctions, *Phys. Rev. B* **50**, 3959 (1994).
- [31] N. Poccia, T. Baturina, F. Coneri, C. Molenaar, X.-J. Wang, G. Bianconi, A. Brinkman, H. Hilgenkamp, A. Golubov, and V. Vinokur, Critical behavior at a dynamic vortex insulator-to-metal transition, *Science (New York, NY)* **349**, 1202 (2015).
- [32] M. Lankhorst, A. Brinkman, H. Hilgenkamp, N. Poccia, and A. Golubov, Annealed low energy states in frustrated large square Josephson junction arrays, *Condensed Matter* **3**, 19 (2018).
- [33] A.-G. Penner, K. Flensberg, L. I. Glazman, and F. von Oppen, Resistivity tensor of vortex-lattice states in Josephson junction arrays, *Phys. Rev. Lett.* **131**, 206001 (2023).
- [34] C. G. L. Böttcher, F. Nichele, J. Shabani, C. J. Palmstrøm, and C. M. Marcus, Dynamical vortex transitions in a gate-tunable two-dimensional Josephson junction array, *Phys. Rev. B* **108**, 134517 (2023).
- [35] See Supplemental Material at <http://link.aps.org/supplemental/10.1103/31zv-84hw> for further details about theoretical methods, device layout and characterization, *IV* characteristics at low magnetic fields, additional data on nonreciprocal depinning current, analysis of the sweep direction dependence and hysteresis effects, a control experiment to demonstrate the role of the diagonal coupling, additional data and data availability statement, which also contains Refs. [55–58].
- [36] J. Shabani, M. Kjaergaard, H. J. Suominen, Y. Kim, F. Nichele, K. Pakrouski, T. Stankevic, R. M. Lutchyn, P. Krogstrup, R. Feidenhans'l, S. Kraemer, C. Nayak, M. Troyer, C. M. Marcus, and C. J. Palmstrøm, Two-dimensional epitaxial superconductor-semiconductor heterostructures: A platform for topological superconducting networks, *Phys. Rev. B* **93**, 155402 (2016).
- [37] M. S. Rzchowski, S. P. Benz, M. Tinkham, and C. J. Lobb, Vortex pinning in Josephson-junction arrays, *Phys. Rev. B* **42**, 2041 (1990).
- [38] C. Baumgartner, L. Fuchs, L. Frész, S. Reinhardt, S. Gronin, G. C. Gardner, M. J. Manfra, N. Paradiso, and C. Strunk, Josephson inductance as a probe for highly ballistic semiconductor-superconductor weak links, *Phys. Rev. Lett.* **126**, 037001 (2021).
- [39] D. Y. Vodolazov and F. M. Peeters, Superconducting rectifier based on the asymmetric surface barrier effect, *Phys. Rev. B* **72**, 172508 (2005).
- [40] D. Suri, A. Kamra, T. N. G. Meier, M. Kronseder, W. Belzig, C. H. Back, and C. Strunk, Nonreciprocity of vortex-limited critical current in conventional superconducting micro-bridges, *Appl. Phys. Lett.* **121**, 102601 (2022).
- [41] Y. Hou, F. Nichele, H. Chi, A. Lodesani, Y. Wu, M. F. Ritter, D. Z. Haxell, M. Davydova, S. Ilić, F. S. Bergeret, A. Kamra, L. Fu, P. A. Lee, and J. S. Moodera, Ubiquitous superconducting diode effect in superconductor thin films *Phys. Rev. Lett.* **131**, 027001 (2023).
- [42] W. F. Schiela, M. Mikalsen, W. M. Strickland, and J. Shabani, Geometric dependence of critical current magnitude and nonreciprocity in planar Josephson junctions *Nat. Nanotechnol.* (2025).
- [43] M. Gupta, G. V. Graziano, M. Pendharkar, J. T. Dong, C. P. Dempsey, C. Palmstrøm, and V. S. Pribiag, Gate-tunable superconducting diode effect in a three-terminal Josephson device, *Nat. Commun.* **14**, 3078 (2023).
- [44] P. Virtanen and T. T. Heikkilä, Nonreciprocal Josephson linear response, *Phys. Rev. Lett.* **132**, 046002 (2024).
- [45] J. F. Steiner, L. Melischek, M. Trahms, K. J. Franke, and F. von Oppen, Diode effects in current-biased Josephson junctions, *Phys. Rev. Lett.* **130**, 177002 (2023).
- [46] R. Wakatsuki, Y. Saito, S. Hoshino, Y. M. Itahashi, T. Ideue, M. Ezawa, Y. Iwasa, and N. Nagaosa, Nonreciprocal charge transport in noncentrosymmetric superconductors, *Sci. Adv.* **3**, e1602390 (2017).
- [47] M. Tinkham, D. W. Abraham, and C. J. Lobb, Periodic flux dependence of the resistive transition in two-dimensional superconducting arrays, *Phys. Rev. B* **28**, 6578 (1983).
- [48] L. Fuchs, D. Kochan, J. Schmidt, N. Hüttner, C. Baumgartner, S. Reinhardt, S. Gronin, G. C. Gardner, T. Lindemann, M. J. Manfra, C. Strunk, and N. Paradiso, Anisotropic vortex squeezing in synthetic Rashba superconductors: A manifestation of Lifshitz invariants, *Phys. Rev. X* **12**, 041020 (2022).
- [49] W. Gillijns, A. V. Silhanek, V. V. Moshchalkov, C. J. Olson Reichhardt, and C. Reichhardt, Origin of reversed vortex ratchet motion, *Phys. Rev. Lett.* **99**, 247002 (2007).
- [50] D. E. Shalóm and H. Pastoriza, Vortex motion rectification in Josephson junction arrays with a ratchet potential, *Phys. Rev. Lett.* **94**, 177001 (2005).
- [51] V. I. Marconi, Rocking ratchets in two-dimensional Josephson networks: Collective effects and current reversal, *Phys. Rev. Lett.* **98**, 047006 (2007).
- [52] J. E. Villegas, S. Savel'ev, F. Nori, E. M. Gonzalez, J. V. Anguita, R. García, and J. L. Vicent, A superconducting reversible rectifier that controls the motion of magnetic flux quanta, *Science* **302**, 1188 (2003).
- [53] C. C. de Souza Silva, J. Van de Vondel, M. Morelle, and V. V. Moshchalkov, Controlled multiple reversals of a ratchet effect, *Nature (London)* **440**, 651 (2006).
- [54] Q. Lu, C. J. Olson Reichhardt, and C. Reichhardt, Reversible vortex ratchet effects and ordering in superconductors with simple asymmetric potential arrays, *Phys. Rev. B* **75**, 054502 (2007).
- [55] V. Ambegaokar and B. I. Halperin, Voltage due to thermal noise in the dc Josephson effect, *Phys. Rev. Lett.* **22**, 1364 (1969).

- [56] M. Tinkham, *Introduction to Superconductivity: Second Edition*, Dover Books on Physics Series, Vol. 1, 2nd ed. (Dover, Mineola, New York, 2004).
- [57] P. Chauhan, C. Thomas, T. Lindemann, G. C. Gardner, J. Gukelberger, M. J. Manfra, and N. P. Armitage, Measurements of cyclotron resonance of the interfacial states in strong spin-orbit-coupled 2D electron gases proximitized with aluminum, [Appl. Phys. Lett.](#) **120**, 142105 (2022).
- [58] G. L. J. A. Rikken, J. A. M. M. van Haaren, W. van der Wel, A. P. van Gelder, H. van Kempen, P. Wyder, J. P. André, K. Ploog, and G. Weimann, Two-terminal resistance of quantum Hall devices, [Phys. Rev. B](#) **37**, 6181 (1988).